Low Yield of Near-Zero-Momentum Electrons and Partial Atomic Stabilization in Strong-Field Tunneling Ionization

Hong Liu,[1] Yunquan Liu,[1,*] Libin Fu,[2,3] Guoguo Xin,[4,5] Difa Ye,[2] Jie Liu,[2,3,4,†] X. T. He,[2,3] Yudong Yang,[1]
Xianrong Liu,[1] Yongkai Deng,[1] Chengyin Wu,[1] and Qihuang Gong[1,‡]

[1]*Department of Physics and State Key Laboratory for Mesoscopic Physics, Peking University, Beijing 100871, China*
[2]*National Key Laboratory of Science and Technology on Computation Physics,*
Institute of Applied Physics and Computational Mathematics, 100088 Beijing, China
[3]*Center for Applied Physics and Technology, Peking University, 100084 Beijing, China*
[4]*School of Science, Beijing Institute of Technology, Beijing 100081, China*
[5]*Department of Physics, Northwest University, Xian, Shaanxi 710069, China*
(Received 22 November 2011; published 27 August 2012)

We measure photoelectron angular distributions of single ionization of krypton and xenon atoms by laser pulses at 1320 nm, $0.2–1.0 \times 10^{14}$ W/cm^2, and observe that the yield of near-zero-momentum electrons in the strong-field tunneling ionization regime is significantly suppressed. Semiclassical simulations indicate that this local ionization suppression effect can be attributed to a fraction of the tunneled electrons that are released in a certain window of the initial field phase and transverse velocity are ejected into Rydberg elliptical orbits with a frequency much smaller than that of the laser; i.e., the corresponding atoms are stabilized. These electrons with high-lying atomic orbits are thus prevented from ionization, resulting in the substantially reduced near-zero-momentum electron yield. The refined transition between the Rydberg states of the stabilized atoms has implication on the THz radiation from gas targets in strong laser fields.

Atomic stabilization in superintense high-frequency fields has been studied theoretically for decades (see, e.g., [1] for a review) and has led to a wealth of profound and intriguing topics in strong-field physics [2–4]. It is usually discussed in the Kramers-Henneberger (KH) frame; i.e., the moving coordinate frame of a free electron responding to the laser field. In the KH frame, the ground-state wave function of the atom splits into two nonoverlapping peaks and the atom becomes stabilized against ionization when the laser frequency is much higher than the bound state frequency of the atom [5]. Recent theoretical investigations further reveal that this concept is not exclusively associated with high frequencies, as widely assumed [6]. The stabilization can also occur when the field frequency is sufficiently large compared to some typical atomic excitation energy. Lacking experimental evidence, this theory is not yet solidified. On the other hand, in an intense low-frequency laser field (e.g., in the infrared regime) the tunneling limit of multiphoton ionization is more appropriately described by the Keldysh theory [7]. With the picture of the Keldysh theory, an effect of ionization suppression associated with tunneling was predicted at some specific field strengths [8]. The controversial issue in the deduction however has been argued recently [9], in which the dependence of the ionization rate on the laser field is found to be monotonic. In contrast to the high-frequency multiphoton ionization, the low-frequency atomic stabilization in the tunneling regime is a more subtle and unsettled question that needs further experimental and theoretical investigation.

In this Letter we present experimental observation that the yield of near-zero-momentum electrons from single ionization of xenon (Xe) and krypton (Kr) atoms produced by a linearly polarized infrared laser is much suppressed in the deep tunneling ionization regime, where the Keldysh parameter γ is much less than unity. Here $\gamma = \sqrt{I_p/2U_p}$, I_p is the ionization potential, U_p is the ponderomotive potential, $U_p = \varepsilon^2/4\omega^2$, ε is the field amplitude, ω is the field frequency, and atomic units (a.u.) are used unless otherwise specified. In the experiment, we did not observe the traditional atomic stabilization in the strict sense that the total ionization yield decreases or at least cease to increase as the laser intensity increases. Instead, we observed that, as the intensity of the field increases, the relative contribution of low-energy photoelectrons to the total ionization yield decreases. With a three-dimensional semiclassical electron ensemble model, we have reproduced this pronounced local ionization suppression effect and uncovered the underlying physics as partial atomic stabilization. We found that, when the electrons initially tunnel in a certain time window at the rising front of a laser cycle, a fraction of atoms can be finally excited into the Rydberg states with high-lying elliptical orbits. Because the frequency associated with the orbit is much smaller than that of the laser, the effect of the fast laser-driven electron oscillations is averaged out on the time scale of the orbital motion and the electrons can remain in the elliptical orbits after the laser pulse is switched off. Those stabilized

atoms can make up the suppressed yield of the low-energy ionized electrons. Our analysis provides an intuitive picture for the low-frequency stabilization in strong-field tunneling ionization that largely extends the ADK (Ammosov-Delone-Krainov) theory [10] and enriches the rescattering scenario [11].

We used linearly polarized 1320 nm radiation generated by an optical parametric amplification system that was pumped by 25 fs, 795 nm pulses from a Ti:Sa laser system with 3 kHz repetition rate, amplified pulse energy up to 0.8 mJ. The estimated pulse duration at 1320 nm was 35–40 fs. The laser intensity was controlled with a pair of polarizers and was calibrated with the electron energy cutoff of 10 U_p.

We measured the photoelectron angular distributions (PADs) with a reaction microscope [12] (for the principle, see [13]). The spectrometer has the photoelectron momentum resolution $\sim$0.02 a.u. along the time-of-flight direction and $\sim$0.05 a.u. along the transverse direction. Ions and electrons were measured with two position-sensitive channel plate detectors, respectively. We applied a weak electric ($\sim$ 3 V/cm) and magnetic ($\sim$ 5 G) field applied along the time-of-flight axis. From the time-of-flight and position on the detectors, the full momentum vectors of particles were reconstructed. In the offline analysis, the photoelectrons were selected in coincidence with their singly charged parent atomic ions. We have carefully adjusted the magnetic field and electrical field along the spectrometer to avoid the poor resolution of the transverse momentum for the low-energy electrons. The laser polarization direction was along the time-of-flight axis.

Figure 1 shows two-dimensional PADs in momentum space (P_z, $P_\perp$) of Xe and Kr in the intensities of 0.2–1 $\times 10^{14}$ W/cm^2 at 1320 nm. The P_z and $P_\perp$ ($P_\perp = \sqrt{P_x^2 + P_y^2}$) represent the momentum parallel and
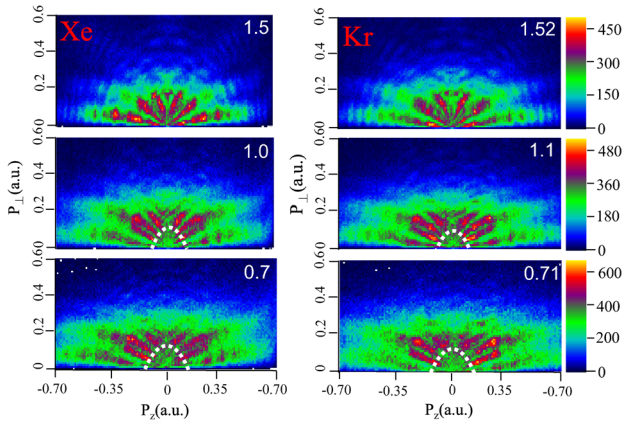
FIG. 1 (color online). Experimental two-dimensional PADs in momentum space (P_z, $P_\perp$) of Kr and Xe in the intensities of 0.2–1 $\times 10^{14}$ W/cm^2 at 1320 nm. The Keldysh parameters are labeled at the top right corner.

perpendicular to the laser polarization axis, respectively. One may first observe the "fanout" structures on the PADs. Indeed, there is a large body of theoretical literature on the origin of resonant structures [14] in the multiphoton ionization regime with both the classical and quantum models [15,16], which is beyond the scope of this Letter. The striking finding in Fig. 1 is that the relative yield of near-threshold electrons is more suppressed when the laser intensity increases.

In order to achieve deep insight into the ionization dynamics behind the striking PADs, we have performed three-dimensional semiclassical electron ensemble simulations including the tunneling effect (for the details see, e.g., [17,18]). Briefly, in the model the electron initial position along the laser polarization direction is derived from the Landau effective potential theory [19]. The tunneled electrons have initially zero longitudinal velocity and a Gaussian-like transverse velocity distribution. Each electron trajectory is weighed by the ADK ionization rate $\varpi(t_0, v_\perp^i) = \varpi_0(t_0)\varpi_1(v_\perp^i)$ [10]. $\varpi_1(v_\perp^i) \propto v_\perp^i \exp \times [\sqrt{2I_p}(v_\perp^i)^2/|\varepsilon(t_0)|]$ is the distribution of initial transverse velocity, and $\varpi_0(t_0) = |(2I_p)^2/\varepsilon(t_0)|^{2/\sqrt{2I_p}-1} \exp \times [-2(2I_p)^{3/2}/|3\varepsilon(t_0)|]$ depends on the field phase ωt_0 at the instant of ionization as well as the ionization potential I_p.

After tunneling, the electron evolution in the combined oscillating laser field and Coulomb field is solved via the Newtonian equation, $\ddot{\vec{r}} = -\vec{r}/r^3 - \varepsilon \cos\omega t \vec{e}_z$, where the polarization direction is along the z axis, r is the distance between the electron and nucleus, ε and ω are the amplitude and frequency of the laser field, respectively. The dressed energy of the electron in an oscillating laser field takes the form of $E = \frac{1}{2}(\dot{\vec{r}} + \frac{\varepsilon}{\omega}\sin\omega t \vec{e}_z)^2 - \frac{1}{r}$. In the simulation, the laser field has a constant amplitude with ten cycles and is ramped off within three laser cycles.

The simulation results of two-dimensional momentum distributions of (P_z, $P_\perp$) for Xe atoms at the intensity of 6×10^{13} W/cm^2 and the wavelength of 1300 nm are presented in Fig. 2(a). Generally, the simulation results agree with the experimental results qualitatively except for the interference patterns. In particular, it reproduces the phenomenon of local ionization suppression in PADs at the origin.

In order to trace the suppressed events, we illustrate the energy distribution of all electrons that tunnel from the first half of the laser cycle $\omega t \in (-\pi/2, \pi/2)$, regardless of whether the final energy is positive or negative, in Fig. 2(c). The figure exhibits that, after the laser pulse there is a large number of tunneled electrons with the final negative energies within $(-0.01, 0)$ a.u., which means that those electrons are finally bounded by the atomic potential. The binding energies of those Rydberg states ($E < 0.01$ a.u.) are much smaller than the photon energy of the low-frequency light (for 1320 nm, the photon energy is $\sim$0.04 a.u.). It has been found experimentally that a large
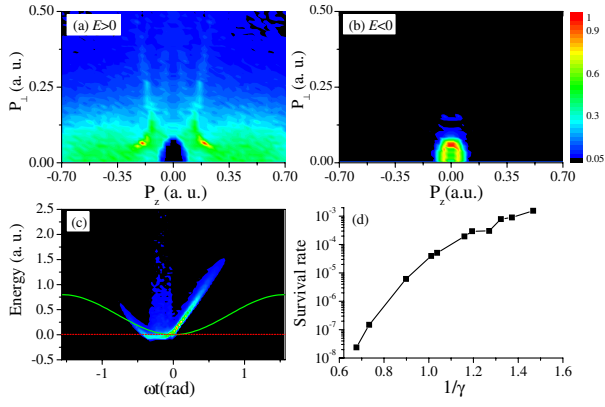
FIG. 2 (color online). Simulation results of two-dimensional momentum distribution (P_z, $P_\perp$) of the ionized electrons (a) and the un-ionized electrons (b) for Xe at the intensity of 6×10^{13} W/cm^2 at 1300 nm. (c) The energy distribution of all electrons vs the initial phase. The solid curve shows the prediction of the simple-man model. (d) The survival rate with respect to the inverse Keldysh parameter.

FIG. 3 (color online). (a) The ionization (or survival) rate vs the initial phase (see the text for details). (b) Two-dimensional momentum distribution (P_z, $P_\perp$) that is contributed from the rising front of the first half laser cycle. (c),(d) show the initial transverse velocities of tunneled electrons with respect to the laser phase that contribute to ionization and stabilization process, respectively. In (d), the solid and dashed curves indicate the theoretical predictions for the boundary for the un-ionized window (see text for details).

number of excited neutral atoms can survive in strong laser fields [20]. In Fig. 2(b), we show the two-dimensional momentum distribution of those electrons with the negative energy (the survival events), which can really make up the suppressed yield of those low-energy ionized electrons. The fact that a substantial part of the tunneled electrons end up in the bound states should affect the momentum spectrum of ionized electrons, particularly the low-energy part. Moreover, the survival rate increases with the inverse Keldysh parameter as presented in Fig. 2(d). This is consistent with the experimental observation that the relative yield of near-zero-momentum electrons is more suppressed in deep tunneling regime.

As shown in Fig. 2(c), in the presence of the Coulomb field, the energies of the electrons released at the rising front of the laser cycle are depressed and the energies of the electrons released at the descending front are enhanced, as compared with the prediction by the simple-man model [21] (the solid curve in Fig. 2(c)]. Some electrons tunneled from the phase region slightly before the field maximum can achieve much higher energy than $2 U_p$ because of the electron chaotic motions [17].

In order to shed more light on the local ionization suppression effect, we now consider the subcycle ionization dynamics. In the combined Coulomb and laser field, the ionization (survival) rate from the first half of the laser cycle is shown in Fig. 3(a). Without the Coulomb field, electrons released from the rising front of the laser cycle will drift away from their parent ions and never return to the vicinity of the nucleus. However, if the Coulomb potential is present, the final ionization rate deviates dramatically from the ADK rate [dashed curve in Fig. 3(a)]. The suppressed ionization results from several distinct phase regions at the rising front of a laser cycle, leading

to the survival rate [solid curve in Fig. 3(a)]. On closer inspection, two-dimensional momentum distribution of (P_z, $P_\perp$) is shown when the electrons are launched within the rising front of the first half laser cycle $\omega t \in (-\pi/2, 0)$ in Fig. 3(b).

To see why those electrons released from those time windows remain un-ionized, we consider the role of the initial transverse velocity $v_\perp^i$ of the tunneled electrons. We show the distributions of the initial transverse velocities of the tunneled electrons that contribute to the ionization rate and survival rate with respect to the field phase in Figs. 3(c) and 3(d), respectively. The launch window of the laser phase and initial transverse velocities for those negative energy electrons consists of a regular hippocampuslike structure (the bright regime in Fig. 3(d)], and an irregular regime [encircled in Fig. 3(d)]. Those electrons ionized slightly before the field maximum with a small transverse velocity are strongly affected by the attraction of the Coulomb field, especially moving with an initially small drift velocity along the laser field.

The physics behind the un-ionized window can be understood by the following approximate theoretical analysis. Considering the Coulomb potential, the final energy of the tunneled electron at the birth time of t_0 can be given by $E_0 = \frac{1}{2}(v_\perp^i \hat{e}_\perp + \frac{\varepsilon}{\omega} \sin\omega t_0 \hat{e}_z)^2 - \frac{1}{|z_0|}$, where $z_0 = \left(I_p + \sqrt{I_p^2 - 4\varepsilon\cos\omega t_0}\right)/2\varepsilon\cos\omega t_0$ is the tunnel exit point. The energy value can be smaller than zero, indicating tunneling without ionization. In Fig. 3(d), the boundary expressed by $E_0 = 0$ in t_0 and $v_\perp^i$ plane is plotted with the solid curve, below which the initial energy of the tunneling electron is negative. Nevertheless, the tunneled electron will be accelerated in the consequent scattering mediated by the Coulomb and light

fields. The energy gain can be expressed analytically by $\Delta E = -\int_{t_0}^{\infty} \frac{z\varepsilon}{\omega r^3} \sin\omega t \, dt$. Ignoring the Coulomb focusing effect, we approximate the electron orbit to be $z = \frac{\varepsilon \sin\omega t_0}{\omega}(t - t_0) + \frac{\varepsilon}{\omega^2}(\cos\omega t - \cos\omega t_0) - z_0$, $r = \sqrt{[v^i_\perp (t - t_0)]^2 + z^2}$, and then the energy change can be obtained by evaluating the above integral numerically. We plot the line of $E_0 + \Delta E = 0$ in Fig. 3(d) (labeled by the dashed line), which gives a good approximation for the boundary that confines the un-ionized window. However, since some electrons inside the *arc* region might experience multiple forward and backward scatterings, their orbits are essentially chaotic [17] and cannot be described by the approximate orbits. During the chaotic scattering, those electrons can acquire additional energy and are eventually ionized, thus making the boundary of the un-ionized window irregular.

Figures 4(a) and 4(b) show the typical trajectories associated with the regular hippocampuslike structure and the irregular structure, respectively, in the specific launching window. The electrons born with a certain field phase and transverse velocity at the rising front of a laser cycle can finally be launched into the elliptical orbits that have the negative energy. In the first optical cycle after tunneling, the electron obtains or releases energy depending on the instantaneous field phases, and then is pumped into the Rydberg elliptical orbits. The difference between those two typical trajectories is that the electron in Fig. 4(a) is ejected directly into an elliptical orbit without collision with the atomic ion. While the tunneled electron in Fig. 4(b) experiences the hard collision with the core during its launching process. Our statistics indicate that the first type orbits constitute ~90% and the second type orbits contribute the residual ~10% of the total un-ionized electrons, respectively.
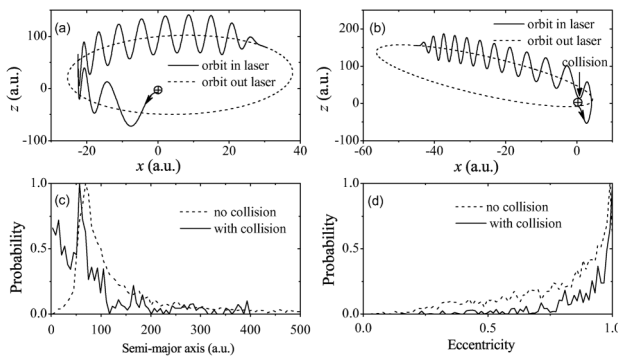
FIG. 4. (a),(b) indicate the typical trajectories in the hippocampuslike structure regime and irregular regime (encircled with solid curve) in Figs. 3(d), respectively. The first type trajectory represents the tunneled electron ejected into the elliptical orbits without collisions, and the second one experiences collisions with nucleus. (c),(d) are the statistical analysis on the semimajor axis and eccentricity distributions corresponding to those two typical trajectories, respectively.

We illustrate the statistic analysis on the semimajor axis and the eccentricity of the elliptic orbits in Figs. 4(c) and 4(d). Those electrons with collisions prefer to move in the elliptic orbits with the smaller semimajor axes and larger eccentricities. The energy of an electron in the elliptic obit is $E = -1/2a$, where a is the semimajor axis. One can find that the distribution of semimajor axis mostly falls into the regime $1/2a \ll \omega$; i.e., the binding energies of the Ryberg states are much smaller than the photon energy. Because the classical elliptic orbit frequencies ($\sim 1/a^{3/2}$) are much smaller than the laser frequency, the fast oscillating motion driven by laser field can be safely averaged out and the electrons will finally remain on the elliptical orbits [see Figs. 4(a) and 4(b)]. This is analogous to the stabilization condition for the Rydberg atoms in the low-frequency light field [5]. However, in our case, the electrons are released from the ground state through tunneling rather than prepared in the Rydberg states directly and thus the stringent atomic stabilization cannot be observed.

With the semiclassical model, we have identified the local ionization suppression as a signature of partial atomic stabilization in the strong-field tunneling ionization regime. The underlying dynamics is that the electrons are dynamically mediated by the Coulomb and light potential in multiple forward and backward scattering processes. Since only the tunneling effect is considered in our semiclassical model, the quantum transition between those Rydberg states is ignored. However, it will efficiently produce the radiation from the allowed transition in the atomic stabilization process. The transition frequency between the Rydberg states is well in THz regime, and thus strong-field atomic stabilization has evident implications on the THz radiation from gas targets in strong laser fields [22], e.g., femtosecond laser filamentation [23].

Note that the above finding differs from the low-energy hump structure of electron spectra observed in the laser polarization direction [24,25], which was attributed as electron multiple forward scattering due to overall influence of the Coulomb potential on the wave packet's longitudinal momentum of the electron [26,27]. This effect results in the enhancement of low-energy photoelectrons in the laser polarization plane. With fully-differential measurement on PADs, we observe that the yield of near-threshold electrons is suppressed in all solid angles.

In conclusion, we have investigated the partial atomic stabilization effect in strong-field tunneling ionization of atoms both experimentally and theoretically. We identify that a fraction of tunneled electrons released in a certain window of the field phase and transverse velocity can be successively launched into two types of elliptical orbits and is finally stabilized there. This leads to the suppressed yield of near-zero-momentum photoelectrons, i.e., a phenomenon that is universal and is very essential in strong-field tunneling ionization. The identification

provides a deep intuition for further quantum control using an attosecond vacuum ultraviolet pulse to excite an atom at a proper time window in a strong few-cycle low-frequency light field.

The semiclassical simulation does not replicate all of the experimental details, e.g., the interference structures. For tunneling ionization at the long wavelength limit, the PADs of low-energy photoelectrons show more or less constant interference structure and we do not observe multiphoton channel closing or channel shift effect. On the other hand, in deep tunneling ionization ($\gamma < 1$) the interference structure in the PADs deviates from the radial distribution. This is very different from the fan structure in multiphoton regime [13,28] (see also Fig. 1 for the largest Keldysh parameter), and a dedicated quantum model is required. Similar to the ionization of the metastable xenon atoms in 7.5 μm far-infrared laser fields [29], these interference structures can be associated with photoelectron holography.

*yunquan.liu@pku.edu.cn

†liu_jie@iapcm.ac.cn

‡qhgong@pku.edu.cn

[1] M. Gavrila, J. Phys. B **35**, R147 (2002).

[2] Q. Su and J. H. Eberly, J. Opt. Soc. Am. B **7**, 564 (1990); J. H. Eberly and K. C. Kulander, Science **262**, 1229 (1993).

[3] M. Dörr, R. M. Potvliege, and R. Shakeshaft, Phys. Rev. Lett. **64**, 2003 (1990).

[4] K. C. Kulander, K. J. Schafer, and J. L. Krause, Phys. Rev. Lett. **66**, 2601 (1991); M. P. de Boer, J. H. Hoogenraad, R. B. Vrijen, L. D. Noordam, and H. G. Muller, Phys. Rev. Lett. **71**, 3263 (1993).

[5] The traditional atomic stabilization requires that the laser frequency is higher than or at least comparable with the bound energy. Recently, the stabilization issue is extended to the Rydberg atoms, e.g., M. V. Fedorov and A. M. Movsesian, J. Phys. B **21**, L155 (1988); B. Piraux and R. M. Potvliege, Phys. Rev. A **57**, 5009 (1998); M. Pont and R. Shakeshaft, Phys. Rev. A **44**, R4110 (1991); S. Askeland, S. A. Sørngård, I. Pilskog, R. Nepstad, and M. Førre, Phys. Rev. A **84**, 033423 (2011).

[6] M. Gavrila, I. Simbotin, and M. Stroe, Phys. Rev. A **78**, 033404 (2008); M. Stroe, I. Simbotin, and M. Gavrila, Phys. Rev. A **78**, 033405 (2008).

[7] L. V. Keldysh, Zh. Eksp. Teor. Fiz. **47**, 1945 (1964) [Sov. Phys. JETP **20**, 1307 (1965)].

[8] R. V. Kulyagin and V. D. Taranukhin, Laser Phys. **3**, 644 (1993).

[9] V. P. Gavrilenk and E. Oks, Can. J. Phys. **89**, 849 (2011).

[10] A. M. Perelomov, V. S. Popov, and V. M. Teren'ev, Zh. Eksp. Teor. Fiz. **52**, 514 (1967) [Sov. Phys. JETP **25**, 336 (1967)]; M. V. Ammosov, N. B. Delone, and V. P. Krainov, Zh. Eksp. Teor. Fiz. **91**, 2008 (1986) [Sov. Phys. JETP **64**, 1191 (1986)]; N. B. Delone and V. P. Krainov, J. Opt. Soc. Am. B **8**, 1207 (1991).

[11] K. J. Schafer, B. Yang, L. F. DiMauro, and K. C. Kulander, Phys. Rev. Lett. **70**, 1599 (1993); P. B. Corkum, Phys. Rev. Lett. **71**, 1994 (1993); P. B. Corkum, Phys. Today **64**, 36 (2011).

[12] Y. Liu, X. Liu, Y. Deng, C. Wu, H. Jiang, and Q. Gong, Phys. Rev. Lett. **106**, 073004 (2011); Y. Liu et al. Phys. Rev. Lett. **104**, 173002 (2010); Y. Deng, Y. Liu, X. Liu, H. Liu, Y. Yang, C. Wu, and Q. Gong, Phys. Rev. A **84**, 065405 (2011).

[13] J. Ullrich, R. Moshammer, A. Dorn, R. Dörner, L. Ph. H. Schmidt, and H. Schmidt-Böcking, Rep. Prog. Phys. **66**, 1463 (2003).

[14] A. Rudenko, K. Zrost, C. D. Schröter, V. L. B. de Jesus, B. Feuerstein, R. Moshammer, and J. Ullrich, J. Phys. B **37**, L407 (2004).

[15] D. G. Arbó, S. Yoshida, E. Persson, K. I. Dimitriou, and J. Burgdörfer, Phys. Rev. Lett. **96**, 143003 (2006).

[16] Z. Chen, T. Morishita, A.-T. Le, M. Wickenhauser, X. M. Tong, and C. D. Lin, Phys. Rev. A **74**, 053405 (2006).

[17] B. Hu, J. Liu, and S. G. Chen, Phys. Lett. A **236**, 533 (1997).

[18] D. Ye and J. Liu, Phys. Rev. A **81**, 043402 (2010).

[19] L. D. Landau and E. M. Lifshitz, *Quantum Mechanics* (Pergamon, New York, 1977).

[20] T. Nubbemeyer, K. Gorling, A. Saenz, U. Eichmann, and W. Sandner, Phys. Rev. Lett. **101**, 233001 (2008).

[21] In the simple-man model, the electron is supposed to release at origin with zero velocity and the subsequent dynamics is described classically without considering Coulomb potential. For details, refer to H. B. van Linden van den Heuvell and H. G. Muller, in *Multiphoton Processes*, edited by S. J. Smith and P. L. Knight (Cambridge University Press, Cambridge, England, 1988); T. F. Gallagher, Phys. Rev. Lett. **61**, 2304 (1988); P. B. Corkum, N. H. Burnett, and F. Brunel, Phys. Rev. Lett. **62**, 1259 (1989).

[22] C. D'Amico, A. Houard, M. Franco, B. Prade, A. Mysyrowicz, A. Couairon, and V. T. Tikhonchuk, Phys. Rev. Lett. **98**, 235002 (2007).

[23] P. Béjot, J. Kasparian, S. Henin, V. Loriot, T. Vieillard, E. Hertz, O. Faucher, B. Lavorel, and J.-P. Wolf, Phys. Rev. Lett. **104**, 103903 (2010).

[24] C. I. Blaga, F. Catoire, P. Colosimo, G. G. Paulus, H. G. Muller, P. Agostini, and L. F. DiMauro, Nature Phys. **5**, 335 (2009); F. Catoire, C. I. Blaga, E. Sistrunk, H. G. Muller, P. Agostini, and L. F. DiMauro, Laser Phys. **19**, 1574 (2009).

[25] W. Quan et al., Phys. Rev. Lett. **103**, 093001 (2009); C. Wu, Y. Yang, Y. Liu, Q. Gong, M. Wu, X. Liu, X. Hao, W. Li, X. He, and J. Chen, Phys. Rev. Lett. **109**, 043001 (2012).

[26] C. Liu and K. Z. Hatsagortsyan, Phys. Rev. Lett. **105**, 113003 (2010).

[27] T. -M. Yan, S. V. Popruzhenko, M. J. J. Vrakking, and D. Bauer, Phys. Rev. Lett. **105**, 253002 (2010).

[28] M. Li, Y. Liu, H. Liu, Y. Yang, J. Yuan, X. Liu, Y. Deng, C. Wu, and Q. Gong, Phys. Rev. A **85**, 013414 (2012).

[29] Y. Huismans et al., Science **331**, 61 (2010).